Micron 39 (2008) 741–748

Contents lists available at ScienceDirect

Micron

journal homepage: www.elsevier.com/locate/micron

Erratum

Comparison of NEXAFS microscopy and TEM-EELS for studies of soft matter☆

Adam P. Hitchcock [a,*], James J. Dynes [a], Göran Johansson [a], Jian Wang [a], Gianluigi Botton [a,b]

[a] Brockhouse Institute for Materials Research (BIMR), McMaster University, Hamilton, ON, Canada L8S 4M1
[b] Canadian Centre for Electron Microscopy (CCEM), McMaster University, Hamilton, ON, Canada L8S 4M1

ARTICLE INFO

Article history:
Received 29 June 2007
Received in revised form 16 August 2007
Accepted 27 September 2007

Keywords:
NEXAFS microscopy
STXM
TEM
EELS
Tomography
Radiation damage

ABSTRACT

In the last 20 years, synchrotron-based soft X-ray microscopy has emerged as a powerful technique for chemical microanalysis. By efficiently measuring near-edge X-ray absorption spectroscopy (NEXAFS) at high spatial resolution, it produces information analogous to that delivered by electron energy loss spectroscopy in a transmission electron microscope (TEM-EELS). NEXAFS microscopy has significant advantages for studies of soft matter, which is typically a challenge for TEM-EELS due to radiation damage. It provides unique capabilities for studying wet samples. Here, we describe current state-of-the-art soft X-ray microscopy instrumentation and techniques (including the recently commissioned spectromicroscopy facility at the Canadian Light Source in Saskatoon), provide brief descriptions of a few recent applications, and make explicit comparisons of the strengths and limitations of NEXAFS microscopy – in particular, scanning transmission X-ray microscopy (STXM) – relative to TEM-EELS for spatially resolved materials analysis by inner shell spectroscopy.

1. Introduction

Analytical transmission electron microscopy (TEM) (Sigle, 2005; Horiuchi and Dohi, 2006; Spence, 2006) is a very powerful tool, particularly with the recent development of aberration compensation optics which significantly improves spatial resolution, and provides much higher efficiencies than previous instruments, particularly for electron energy loss spectroscopy (EELS). However, it is always a challenge to use TEM, and especially TEM-EELS for studies of soft matter, since virtually all samples of this type – polymers, unfixed biological systems, etc. – are extremely sensitive to radiation damage. In the last 20 years, several synchrotron-based, soft X-ray microscopy techniques have been developed and optimized for studies of soft matter (Kirz et al., 1995; Ade, 1998; Ade and Urquhart, 2002; Hitchcock et al., 2005; Ade and Hitchcock, in press). These techniques provide compositional and chemical structure analysis analogous to that delivered by TEM-EELS, albeit at lower spatial resolution, through spatially resolved near-edge X-ray absorption spectroscopy (NEXAFS). NEXAFS microscopy has significant advantages for studies of orientation in soft matter samples, and has unique capabilities to examine fully wet samples. In this short review, we outline the state-of-the-art in soft X-ray microscopy techniques, present the recently commissioned spectromicroscopy facility at the Canadian Light Source (CLS) in Saskatoon (Kaznatcheev et al., 2004, 2007), and use examples from environmental biology and polymer science to illustrate the strengths and limitations of NEXAFS microscopy relative to TEM-EELS.

2. Transmission X-ray microscopy instrumentation and capabilities

Fig. 1 presents schematics of the two main types of soft X-ray transmission microscopes while Table 1 lists locations of existing and planned devices. The full field variant was developed first (Schmahl et al., 1980) and is called transmission X-ray microscopy (TXM). In TXM unmonochromated light from a bend magnet at a synchrotron is partially monochromated by a Fresnel zone plate (Attwood, 2000) acting as a condenser, and focused to a ~10 μm spot at the sample. X-rays that are transmitted are imaged using a second imaging zone plate and the image is recorded with a charge-coupled device (CCD) camera using typical exposures from 0.1 to 10 s. Tessellation is required to measure areas larger than ~10 μm in diameter. The spectral capabilities of TXM are quite limited since the ZP has a resolving power of ~100 and the line shape is far from Gaussian, and has long tails. Another

DOI of original article: 10.1016/j.micron.2007.09.008
☆ This paper was mistakenly published in Volume 39, Issue 3 so is re-printed here with the special issue it belongs to.
* Corresponding author.
E-mail address: aph@mcmaster.ca (A.P. Hitchcock).

0968-4328/$ – see front matter © 2008 Elsevier Ltd. All rights reserved.
doi:10.1016/j.micron.2007.09.010

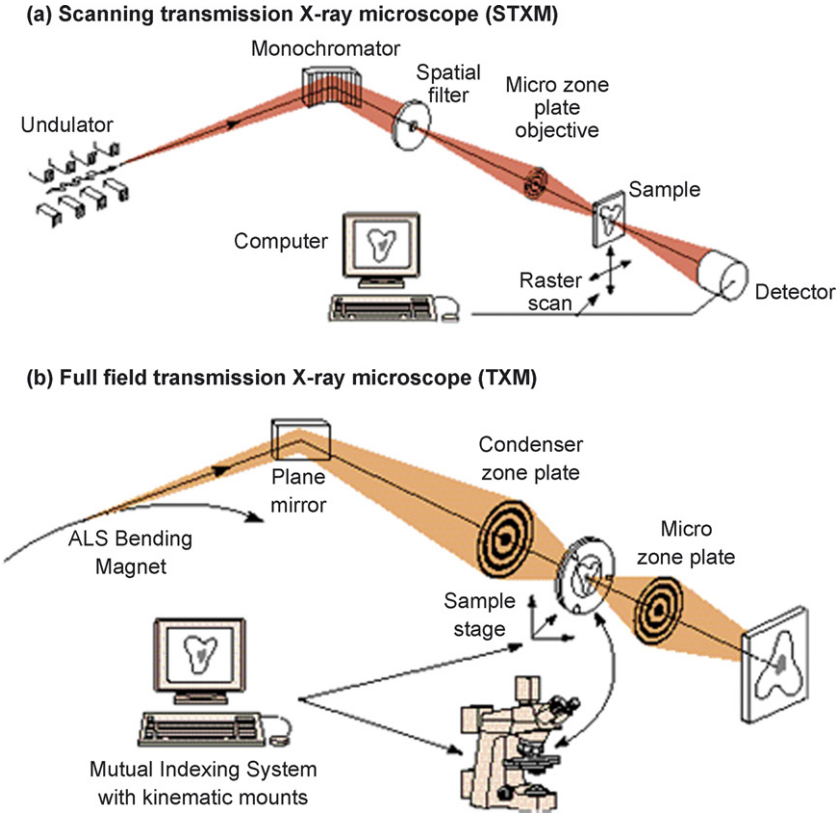

Fig. 1. Schematics of the two main types of soft X-ray zone plate based microscopes. (a) Scanning transmission X-ray microscopy (STXM); (b) full field transmission X-ray microscopy (courtesy of ALS, LBNL).

disadvantage of TXM is that there is a ZP after the sample which is a low efficiency optic (10–15% transmission). This means 5–10 times more photons must pass through the sample for a given quality of measurement, which increases the integrated dose without improving the result. TXM has contributed significantly in the fields of imaging unstained, intact biological samples (Larabell and Le Gros, 2004) and in magnetism (Fischer et al., 2001). The rapid data acquisition has been exploited for kinetic studies (Fischer et al., 2001), and for tomography of biological samples (Larabell and Le Gros, 2004).

The second type, scanning transmission X-ray microscopy (STXM), was developed first by Kirz and Rarback (1985). In STXM a conventional high-resolution synchrotron beamline is used to provide high brightness, partially coherent illumination of a Fresnel zone plate. The sample is placed at the focus of the zone plate and raster scanned while detecting the transmitted X-rays, using either single photon counting or current detection. Relative to TXM it has significant advantages for microanalysis because it has high spectral resolution, typically $E/\Delta E \geq 3000$, ease of scanning over a wide range of photon energies (current TXM instruments typically require tedious manual adjustments when changing from one core edge to another), and better efficiency with respect to radiation damage, since the only inefficient optic is located before the sample. Modern STXMs (Feser et al., 2000; Kilcoyne et al., 2003) have sophisticated mechanical scanning and interferometry based control systems which provide large ranges

Table 1
Locations and properties of soft X-ray (<3000 eV) transmission X-ray microscopes

Type	Facility	Location	Source	E-range (eV)	Status
TXM	Ritsumeikan BL12	Kyoto, Japan	ZP condenser	500	Operating
TXM	Bessy U41TXM	Berlin, Germany	ZP condenser	500	Operating
TXM	ALS TXM	Berkeley, CA, USA	ZP condenser	250–900	Operating
TXM	Astrid	Aarhus, Denmark	ZP condenser	500	Operating
TXM	ALS, NCXT	Berkeley, CA, USA	ZP condenser	250–9000	Commissioning
STXM	NSLS X1A (2 STXMs)	Upton, NY, USA	Undulator	250–1000	Operating
STXM	Bessy	Berlin, Germany	BM	250–750	Operating
STXM	ALS 5.3.2	Berkeley, CA, USA	BM	250–750	Operating
STXM	ALS 11.0.2	Berkeley, CA, USA	EPU	100–2000	Operating
STXM	SLS	Villigen, Switzerland	BM	250–750	Operating
STXM	CLS 10ID1	Saskatoon, Canada	EPU	250–2500	Operating
TXM and STXM	Elettra Twin-mic	Trieste, Italy	Undulator	250–2000	Operating
STXM	Bessy	Berlin, Germany	EPU	250–1500	Construction
STXM	SSRL	Stanford, CA, USA	EPU	250–1500	Construction
STXM	Soleil	Paris, France	EPU	250–1500	Design
STXM	SSRF	Shanghai, China	Undulator	250–2000	Design

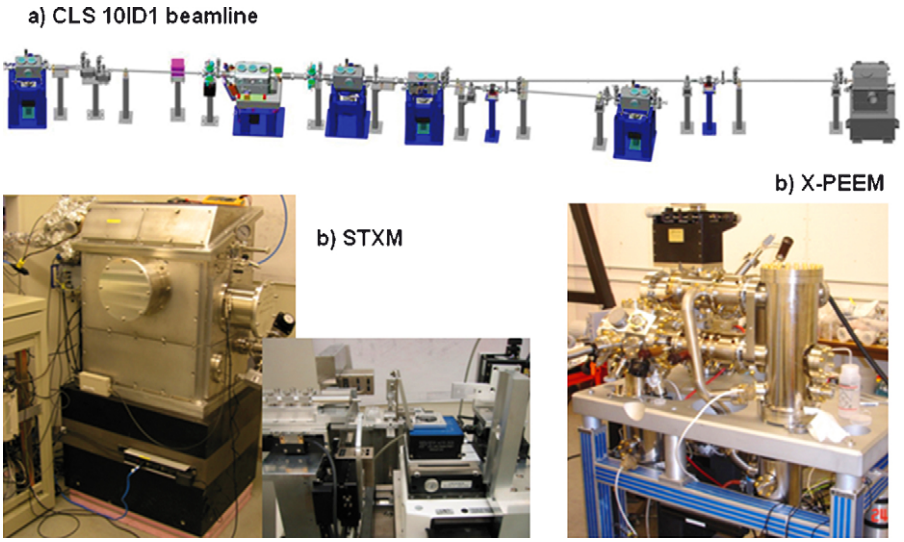

Fig. 2. Schematic of the CLS spectromicroscopy facility. The source (not shown) is an Apple type II elliptically polarized undulator (EPU), located to the left of the elements displayed, with its centre 15 m from the first element shown (the M1 tank). In order from left to right, the elements are: the M1 mirror tank, the plane grating monochromator (PGM) containing the M2 mirror and three gratings, the M3PEEM mirror which is translatable to allow light to pass straight into the M3STXM mirror. The last blue element on the right is the M4PEEM refocusing mirror. The X-PEEM is not shown but it is positioned such that the sample is about 50 cm downstream from the exit of the M4PEEM tank. (For interpretation of the references to color in this figure legend, the reader is referred to the web version of the article.)

of sample scanning (from sub-micron to several cm) with high precision. However, acquisition is slower than TXM—typical dwell times are ~1 ms/pixel, resulting in a scan time for a 200 pixel × 200 pixel image of 40 s. A number of excellent reviews (Ade, 1998; Ade and Urquhart, 2002; Kirz et al., 1995; Howells et al., 2007) can be consulted for more technical details on the optics and mechanics of transmission X-ray microscopes.

Recently the soft X-ray spectromicroscopy facility at the CLS has been commissioned and is now available to general users. The beamline layout is shown in Fig. 2. Its source point is an elliptically polarized undulator (EPU) which can deliver fully circular polarized light (250–900 eV), as well as elliptical and fully linear polarized light with the ability to rotate the E-vector of the light over a range of −90° to 90°. X-rays from the EPU are directed by a sagittal cylindrical mirror into a plane grating monochromator (PGM) (Kaznatcheev et al., 2004) with a virtual entrance slit and dispersion in the vertical direction. There are three stripes on a single grating substrate providing optimal performance over the full photon energy range from 200 to 2500 eV as well as phase space matching for the STXM branch. After the PGM, the beamline splits into two branch lines and toroidal mirrors are used to focus the light into each of the two experimental end stations. One branch is relatively short, and is used for X-ray photoemission electron microscopy (X-PEEM). The other branch is long to enable a single diffraction mode of operation for a dedicated STXM. The beamline and STXM have been shown to perform similarly to the STXM at beamline 11.0.2 at the Advanced Light Source (ALS), on which it was modeled.

3. Comparison of STXM and TEM-EELS

To be useful for chemical microanalysis, a technique should operate at the highest possible spatial resolution, have strong chemical sensitivity which can be interpreted either on fundamental grounds or with the aid of reference spectra ('fingerprint' mode), and be adapted to a wide range of sample types. Both STXM and TEM-EELS fulfill these requirements, but with different emphases.

At present the very best spatial resolution achieved in X-ray microscopy is 15 nm (Chao et al., 2005), which is more than two orders of magnitude worse than the best TEM spatial resolution. There are six STXMs in the world operating routinely with spot sizes well below 50 nm. The energy resolution of most NEXAFS microscopes is better than 0.1 eV, a value only achieved for core-loss EELS in TEM using high-resolution monochromators. Historically, even with a monochromator, it has been a challenge to achieve energy resolutions better than perhaps 0.2 eV in the core loss region due to the difficulty of maintaining instrument conditions sufficiently stable for long enough time to acquire adequate statistics. However, recent dramatic improvements in electron microscope power supplies and control strategies have lead to modern instruments with sufficient stability to take advantage of incident beam monochromatization.

Perhaps even more challenging for TEM-EELS, particularly when studying soft matter such as polymer or biological samples, is acquiring spectra at high spatial resolution without spectral distortion by radiation damage. Radiation damage per unit of analytical information has been shown to be typically 100–1000 times lower in NEXAFS microscopy than in TEM-EELS (Rightor et al., 1997). This difference arises mainly because a very large fraction of electron energy losses are damaging (bond breaking occurs for almost all loss events above the first ionization potential of the system) but only the small subset of energy losses associated with core level excitation are analytically useful. In contrast, in photoabsorption every photon that is absorbed contributes to the analytically useful spectrum, and thus the information per unit damage is higher.

For chemical analysis of biological samples by TEM-EELS it is important that the ultrastructure be preserved and that few or no chemical treatments are used. The TEM community has developed sophisticated techniques for rapid freezing and examination of frozen hydrated biological samples with TEM-EELS (e.g. Leapman and Sun, 1995). These techniques are also being used for cryo-STXM (Wang et al., 2000), and cryo-TEM (Larabell and Le Gros, 2004), although all the results presented here were recorded at room temperature. The TEM-EELS community has also implemented environmental control systems which allow studies of hydrated samples at room temperature or with in situ interaction with controlled gaseous environments. Daulton et al. (2002) have used such techniques to study Cr reduction and biomineralization

by bacteria. Similar approaches are being implemented in STXM (Hanhan et al., 2007). Typically elemental and oxidation state mapping in energy filtered TEM (a direct analog to the image sequence technique in NEXAFS microscopy) achieves a spatial resolution well below 10 nm and an elemental sensitivity of 0.5 at.% in any column through the sample (Sigle, 2005; Horiuchi and Dohi, 2006). Corresponding figures for STXM are a spatial resolution better than 30 nm and a typical sensitivity for chemical components of 1% of the total thickness in any column, although selected cases where higher doses can be used have pushed that limit to ~0.1%, for example in the studies of magnetization dynamics of a 4 nm thick Co layer (100 nm × 150 nm lateral dimension) buried in a 3 μm thick spin injection structure (Acremann et al., 2006).

A powerful capability of TEM-EELS is the use of the low loss region (2–40 eV) for spectroscopy and energy filtered imaging (Libera and Disko, 2004). Since the cross-sections are very high in this region, high quality results can be obtained rapidly with very low doses, thus minimizing radiation damage and reducing the need for long-term power supply stability. Very elegant low loss TEM-EELS studies of water mapping in hydrated polymer systems (Sousa et al., 2006a) and protein adsorption on polymer blends (Sousa et al., 2006b) have been published recently. There is no direct counterpart of this technique using synchrotron radiation although laser absorption and fluorescence microscopy techniques do provide similar analytical information in the visible and UV spectral ranges, but at much lower spatial resolution.

4. Selected examples of NEXAFS microscopy with STXM

4.1. Wet samples—biofilms

A unique advantage of STXM and TXM is the ability to study fully hydrated samples. This capability has been exploited extensively in studies of wet biofilms (Lawrence et al., 2003; Dynes et al., 2006a,b) and in situ electrochemistry (Guay et al., 2005). For the past 4 years the ALS STXMs have been used extensively to explore natural (multiple species) and cultured (single species) microbial biofilm systems. An important aspect has been developing correlative microscopy techniques to allow the same region of a sample to be examined by STXM, TEM, TEM-EDX, and confocal laser scanning microscopy (CLSM) (Lawrence et al., 2003). With this approach we have examined the concentration of metals in biofilms, with an emphasis on differentiating active (biologically assisted) and passive (intrinsic chemical affinity) mechanisms of concentrating specific metal ions (Dynes et al., 2006a). Another area of current interest is tracking the locations of antimicrobial compounds in bacterial biofilms in order to study antimicrobial resistance phenomena (Dynes et al., 2006b). The example presented here involves use of a new window material to make biofilm wet cells. The 30 nm thick polyimide windows (Luxel Corporation, Friday Harbor, WA, http://www.luxel.com/) are a significant improvement over the silicon nitride windows which are typically used. The polyimide is much more robust (the Si_3N_4 windows are very brittle), and, although they have high carbon content, the absorbance of 60 nm of polyimide window is less than 0.6 everywhere in the C 1s region (280–300 eV) whereas the OD for two 75 nm Si_3N_4 windows is such that the window absorbance is more than 1.3 in this same energy range. The much reduced absorbance by the polyimide windows means that thicker samples can be used before distortions from absorption saturation become a problem.

A river biofilm (inoculation from the South Saskatchewan river) was grown for 8 weeks on a polycarbonate slide in a rotating annular reactor (Lawrence et al., 2000), after which the biofilm was aseptically scraped from the entire slide (11 cm^2) with a silicone spatula and placed in a sterile 1-mL centrifuge tube. An aliquot of the biofilm material was placed onto a 1 mm diameter Luxel polyimide membrane and a second polyimide membrane was aligned and placed on top of the wet biofilm. The polyimide sandwich (wet cell) was then sealed with epoxy and examined by STXM. Fig. 3 shows images and chemical analysis of this sample. The 288.2 eV transmission image (Fig. 3a) highlights the microbial entities in the biofilm since the signal at 288.2 eV is dominated by the strong C 1s → $\pi^*_{C=O}$ band of the amide carbonyl carbon of protein, although there are also weak contributions from the carbonyl carbon of lipids and C–H signal of polysaccharides. An area of the biofilm was studied in detail by collecting a C 1s image sequence (280–320 eV) over a 20 μm × 20 μm area. The image sequence consisted of 93 images (360 pixels × 360 pixels, 55 nm pixel size), and a dwell time of 1 ms/pixel (total acquisition time of 4 h). After the STXM measurements (~8 h in an ultra dry He atmosphere of the STXM), the biofilm was still fully hydrated as indicated by interference colors in an optical image measured after removing the sample (Fig. 3b). From the optical image it is apparent from the wrinkles that the polyimide has conformed to the biofilm. This type of stress frequently leads to cracks or breakage of silicon nitride windows, which often complicates (due to drying through cracks) or prevents (due to breakage) studies of fully hydrated samples. Quantitative maps of protein, lipid, polysaccharide, carbonate and K^+ were derived from the C 1s image sequence by fitting the spectrum at each pixel to a linear combination of the spectra of expected components (protein, polysaccharide, lipid, K^+, CO_3^{2-}) which were reported previously (Dynes et al., 2006a,b). Fig. 3c–g shows the component maps for protein, lipid, polysaccharide, carbonate and K^+. The grey scales are quantitative in terms of thickness of each component. Fig. 3h displays a color composite map of protein, polysaccharides and lipids. The biofilm was composed mainly of protein and polysaccharides, with the protein and lipids mainly attributed to bacterial cells while the polysaccharides indicated locations of extracellular polymeric substances. The carbonates and K^+ mainly occurred as discrete particles, with some of these associated with lipids. Ca^{2+} and Fe^{3+} signals were also mapped in this same region.

4.2. Wet samples—tomography

In addition to two-dimensional projection, it is possible to use serial section or angle-scan tomography to provide three-dimensional imaging with electron or X-ray microscopy. Both serial section (Fiala, 2005), and angle-scan tomography (Mastronarde, 1997) methods are well developed in electron microscopy. Cryo-tomography of biological samples is being performed extensively using full field TXM (Larabell and Le Gros, 2004). The National Centre for X-ray Tomography (NCXT), which provides cryo-TXM over a wide range of X-ray energies, has recently been commissioned at the ALS. Both serial section tomography (Hitchcock et al., 2003) and angle-scan cryo-tomography (Wang et al., 2000) have been demonstrated using scanning transmission X-ray microscopy. It is important to note that radiation damage rates in fully hydrated specimens examined in liquid water are much higher than the damage rates when the same sample is frozen due to suppression of damage associated with hydroxyl radicals which are immobilized in frozen specimens (London et al., 1992). At the same time, if the goal is chemical characterization by NEXAFS spectromicroscopy, measuring frozen specimens only improves morphological stability, not chemical stability since the rate of damage as measured by spectral change has been shown to be the same at 77 and 300 K (Beetz and Jacobsen, 2003).

Recently, we have extended STXM to acquire tomograms from room temperature wet samples at multiple photon energies,

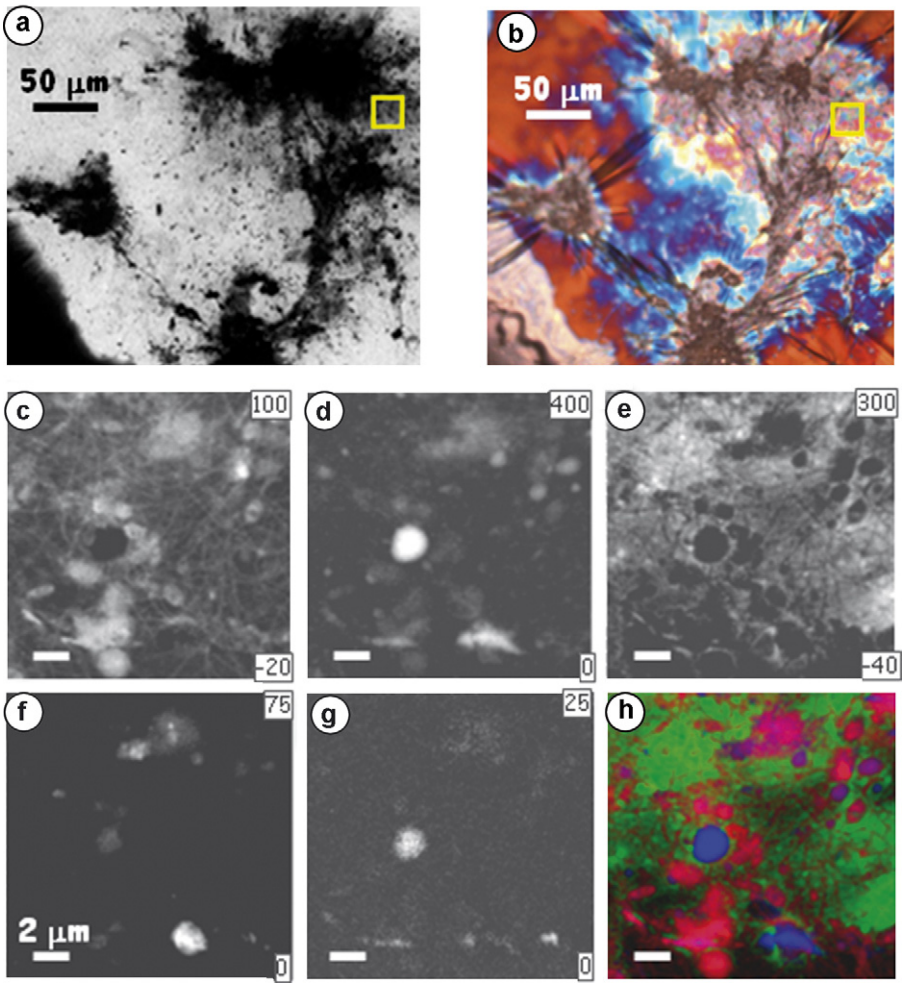

Fig. 3. (a) Transmission image (288.2 eV) of a river biofilm recorded by scanning transmission X-ray microscopy (STXM). (b) Optical image recorded after the STXM study. The yellow rectangle in (a and b) shows the area studied with a C 1s image sequence (280–320 eV). Component maps of the detailed study area derived by curve fit of the spectrum at each pixel to quantitative reference spectra. (c) Protein, (d) lipid, (e) polysaccharide, (f) CO_3^{2-}, and (g) K^+. The numbers to the left of each component map are the lower and upper bounds of the grey scale indicating thickness in nanometres at each pixel. (h) Color coded composite map of selected (rescaled) components (c–g), red: protein, green: polysaccharide and blue: lipids. (For interpretation of the references to color in this figure legend, the reader is referred to the web version of the article.)

thereby using the spectral signal in conjunction with angle-scan tomography to achieve three-dimensional chemical mapping with NEXAFS microscopy for the first time (Johansson et al., 2007). Hollow latex particles prepared by multi-stage emulsion polymerization techniques (McDonald and Devon, 2002) are being developed for use as paper coatings (opacifying agents, glossing aids) and other purposes. The properties of these particles can be fine tuned for particular applications by controlling the interior structure, which can vary from highly dense with polymer struts, to completely hollow (Beach et al., 2005). We have applied STXM chemical tomography to ~1 μm diameter polystyrene latex microspheres filled with a low-density polyacrylate (Johansson et al., 2007). The microspheres were contained in a 4–5 μm diameter thin walled glass capillary which was measured in STXM with *x*–*y* sample raster scanning to form images in the usual fashion. Fig. 4a is a cartoon of the sample and quantitative spectra of the key chemical components, polystyrene, polyacrylate and water. Fig. 4b presents renderings of the three-dimensional chemical structure derived from complete tomograms (36 angles from 0° to 180°), recorded at two photon energies (530.0 and 532.2 eV in the pre-O 1s edge region. Full details of the acquisition and data analysis are presented elsewhere (Johansson et al., 2007). The grey scale component of the rendered image, derived from the 530.0 eV signal, displays the capillary wall and the PS shell of the microspheres. The green and blue signals indicate the three-dimensional distribution of the polyacrylate, and are derived from the difference in the 532.2 and 530.0 eV signals. In this sample, much of the polyacrylate has in fact leaked from the microspheres. Some microspheres were found to be empty, while others were completely filled with polystyrene. Detailed analysis of these results provides very useful feedback which could be used to further optimize the fabrication process. To our knowledge this is the only way of getting detailed, chemically specific spatial information on a relatively dilute (<5% of solids) encapsulated component in an aqueous suspension, without adding uncertainties associated with drying and sectioning. Very recently, we have extended this technique even further by achieving chemical tomography at the C 1s edge (Hitchcock et al., submitted for publication).

4.3. Molecular orientation

Another area where both NEXAFS microscopy and TEM-EELS provide useful analytical information is molecular orientation in anisotropic systems through the dependence of the intensities of specific spectral features on the direction of the momentum

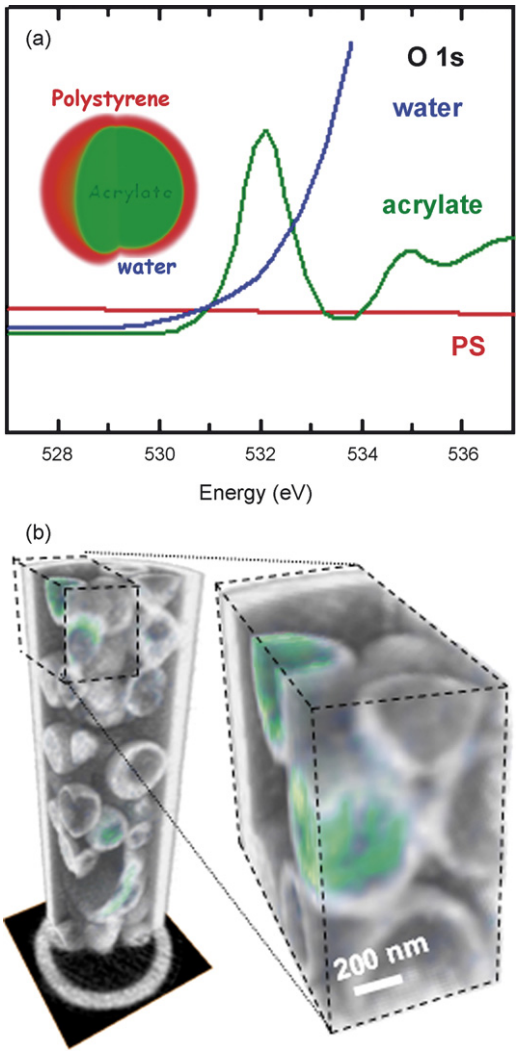

Fig. 4. (a) Schematic of the sample and pre-edge O 1s spectra of components. (b) Reconstruction from 2-energy STXM angle-scan tomogram (grey: polystyrene, glass; green: polyacrylate). Sample courtesy Mindy Keefe, Gary Mitchell, Dow Chemical (from Johansson et al., 2007). (For interpretation of the references to color in this figure legend, the reader is referred to the web version of the article.)

transfer vector (EELS) or the electric vector (NEXAFS). For example, the q-dependence of electron energy loss in TEM has been used to explore the structure of single walled carbon nanotubes (Stéphan et al., 2001) and to investigate metal–nanotube bonding (Jin-Phillipp and Rühle, 2004) on a near atom-by-atom basis. While X-ray microscopy cannot (and is very unlikely ever to) compete with the high spatial resolution of modern TEM, it does offer some attractive advantages for studies of orientation. It is much easier to experimentally control the angular relationship between the E-vector of the light and a given spatial direction on the sample in X-ray microscopy than in TEM-EELS. On bend magnet and linear undulator beamlines this is achieved by manipulating the sample in space relative to a fixed E-vector. In beamlines equipped with an EPU such as the CLS spectromicroscopy line, the E-vector can be rotated by changing the phase of the EPU. This allows studies of in-plane (azimuthal) alignment, and also out-of-plane (polar) alignment, when combined with a tilted sample mount and scanning at an angle relative to the X-ray propagation direction (typically 30°). Studying alignment in partially or fully hydrated samples is also possible. The ALS 5.3.2 bend magnet STXM has been used to map β-sheet regions in natural silk fibers (Hernández-Cruz et al., 2006, 2007; Rousseau et al., 2007) by spatially resolved linear dichroism of the C 1s → π^*_{amide} transition. This study involved comparisons of two different types of silk—from the cocoon of *Bombyx mori* silk worms, and from the draglines of *Nephia clavipes* spiders. The dependence of the alignment structure on the spinning speed of *N. clavipes* spider silk was also investigated. The individual β-sheet crystallites are 5–10 nm in size, as determined by X-ray scattering and directly imaged using low voltage TEM (Drummy et al., 2006). While STXM cannot resolve the individual β-sheet crystallites, there are inhomogeneous groupings of them which are also important with regard to the structure–properties relationships in silk. The STXM results allowed quantitative evaluation of the distribution of orientation over large areas of fiber, giving information that complements X-ray and TEM studies. The results were directly compared with quantitative Raman analysis of orientation on a single fiber basis and good agreement of the dependence of the average degree of orientation on the spinning speed was found between the STXM and Raman measurements (Rousseau et al., 2007).

4.4. Radiation damage

Radiation damage is an issue for both TEM-EELS and NEXAFS microscopy since both techniques use ionizing radiation. Much effort has been spent using both techniques to characterize mechanisms and rates of radiation damage. Recently we have revisited our earlier work comparing inelastic electron scattering versus X-ray absorption for inner shell excitation (Rightor et al., 1997) which evaluated the impact of radiation damage in the two techniques, using a figure of merit in terms of analytical information from inner shell spectroscopy per unit of radiation damage. In that work the radiation damage and its spectral characterization were done at the same time, using each technique independently of the other. TEM-EELS was used to evaluate the dose–damage relationship for electron impact, while a non-imaging NEXAFS system was used to evaluate the dose–damage relationship for X-ray absorption. Here we have improved on the earlier work in three important aspects. (1) We are now using the highly focused X-ray beam of the STXM (35 nm) rather than a spectroscopy beamline (∼1 mm) and thus the dose density and dose rates are much higher. (2) The analysis of the spectral changes was done with the same spectrometer (STXM) for both electron and X-ray damage. This reduces possible inconsistencies associated with comparing TEM-EELS and NEXAFS. (3) For the first time the spectral changes caused by electrons were measured at lower doses than can be achieved to get a TEM-EELS spectrum (see Fig. 5a).

We systematically damaged a thin film microtomed sample of polyethylene terephthalate (PET) by variable time exposure to a defocused electron beam in a TEM (JEOL2010F) and by variable time exposure to focused, 320 eV X-rays in STXM. We then used STXM to quantify the dose–damage relationship as well as radiation damage spreading from each irradiation. Fig. 5 presents C 1s spectra recorded by TEM-EELS and STXM, images of the damaged polymer, and the dose–damage curves for the electron and X-ray cases. A quantitative analysis of the dose–damage curves yielded critical dose values of 380 ± 50 and 460 ± 50 MGy for the electron impact and X-ray damage, respectively. These values are similar to those reported earlier (Rightor et al., 1997). The observation that the critical dose for damage to the carbonyl functional groups of PET by electrons and X-rays is essentially the same indicates that secondary processes (low energy electron, ion or radical chemistry) rather than the initial primary event (inner shell excitation by inelastic X-ray scattering or X-ray absorption), dominate the radiation damage and thus determine the chemical changes and

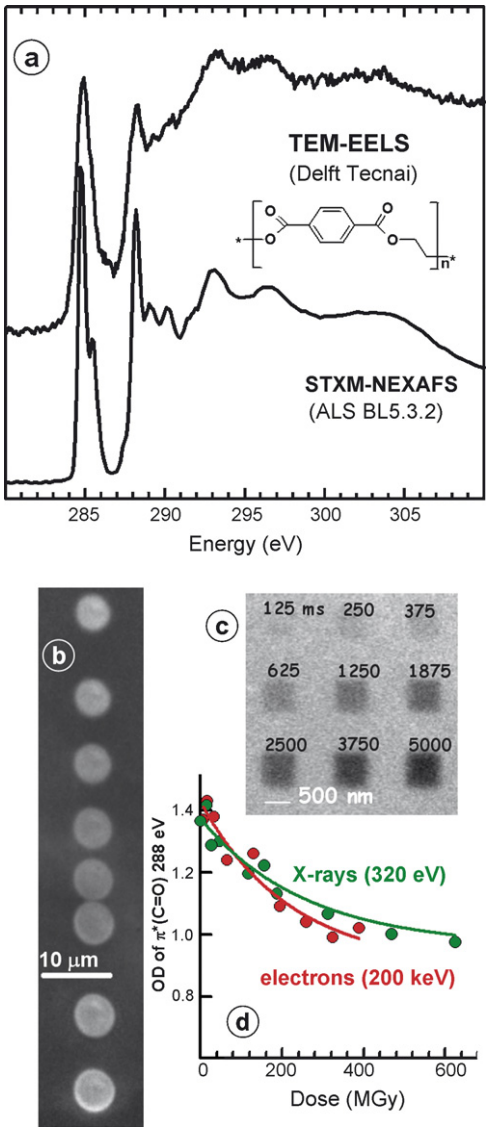

Fig. 5. (a) Comparison of C 1s spectra of PET, recorded by monochromated TEM-EELS (Delft Tecnai) and by STXM (ALS STXM5.3.2). STXM images (288.3 eV, the $\pi^*_{C=O}$ band) of systematic damage by (b) a defocused 200 keV electron beam in a JEOL2010F (exposure times were 2, 5, 10, 20, 40, 60, 80, 100 s at a current of 63 pA) and (c) 320 eV X-rays, at an incident flux of 4.1 MHz with exposure per 60 nm pixel of the indicated times (ms). (d) Comparison of dose–damage curves for electrons and X-rays.

the critical dose. On the basis of the same figure of merit used previously, namely acquiring spectra of a single core level over a 40 eV energy range, we determine a 100–500-fold advantage for using X-ray microscopy relative to TEM-EELS. This is readily understood from the fundamental physics of the two processes. In electron impact almost all electron energy losses are damaging (essentially all losses above the first ionization potential of the system) but only the small subset of energy losses associated with inner shell excitation are analytically useful. For a 40-eV spectral range at the C 1s edge this is a percent or less of the total loss cross-section. The fraction of the signal is even smaller for higher energy inner shell edges. In contrast, in photoabsorption every photon that is absorbed contributes to the inner shell spectrum, and thus the analytically useful information provided per unit damage is higher. The advantage for X-rays with regard to relative information/unit damage is clearly greater at higher transition energies, especially since electron energy loss cross-sections fall off much faster with increasing transition energy than X-ray absorption cross-sections (Egerton, 1996). In contrast, due to the capability of many TEM-EELS spectrometers to simultaneously acquire signal over large spectral ranges via parallel detection, if the criterion is changed to widen the spectral range required for problem solving, there is less advantage of X-ray over electron energy loss techniques.

5. Summary

Both TEM-EELS and NEXAFS microscopy are extremely powerful techniques for spatially resolved elemental and chemical analysis based on inner shell spectroscopy. Clearly TEM-EELS is far superior with regard to spatial resolution and will remain so since the far field resolution limit for X-ray imaging at the C 1s edge is 4 nm. At present there is some advantage in terms of spectral quality (energy resolution and statistics) for inner shell spectra recorded with X-ray absorption, but this advantage is being reduced with the more efficient aberration compensated instruments. With regard to radiation damage and studies of wet samples, X-ray microscopy techniques have a clear advantage. The wise materials analyst will endeavor to have access to both techniques and exploit the specific advantages of each one as required by the problem at hand.

Acknowledgements

We thank S. Lazar for assistance with recording the TEM-EELS spectrum of PET. Research supported by NSERC, CFI and Canada Research Chair. STXM measurements were carried out at beamline 5.3.2 at the Advanced Light Source which is supported by the Office of Basic Energy Sciences of the U.S. Department of Energy under contract DE-AC03-76SF00098. The Canadian Light Source is supported by NSERC, CIHR, NRC and the University of Saskatchewan. We thank David Kilcoyne and Tolek Tyliszczak for their expert support of STXM5.3.2 and Konstantine Kaznatcheev, Chithra Karunakaran and Martin Obst for their support of the CLS STXM.

References

Acremann, Y., Strachan, J.P., Chembrolu, V., Andrews, S.D., Tyliszczak, T., Katine, J.A., Carey, M.J., Clemens, B.M., Siegmann, H.C., Stöhr, J., 2006. Time resolved imaging of spin transfer switching: beyond the macrospin approximation. Phys. Rev. Lett. 96, 217202.

Ade, H., 1998. X-ray spectromicroscopy. In: Samson, J.A.R., Ederer, D.L. (Eds.), Experimental Methods in the Physical Sciences, vol. 32. Academic Press, NY, pp. 225–262.

Ade, H., Hitchcock, A.P., in press. NEXAFS microscopy and resonant scattering: composition and orientation probed in real and reciprocal space. Polymer.

Ade, H., Urquhart, S.G., 2002. NEXAFS spectroscopy and microscopy of natural and synthetic polymers. In: Sham, T.K. (Ed.), Chemical Applications of Synchrotron Radiation. World Scientific Publishing, Singapore, pp. 285–355.

Attwood, D., 2000. Soft X-rays and Extreme Ultraviolet Radiation, Principles and Applications. Cambridge University Press.

Beach, E., Keefe, M., Heeschen, W., Rothe, D., 2005. Cross-sectional analysis of hollow latex particles by focused ion beam-scanning electron microscopy. Polymer 46, 11195–11197.

Beetz, T., Jacobsen, C., 2003. Soft X-ray radiation-damage studies in PMMA using a cryo-STXM. J. Synchrotron Radiat. 10, 280–285.

Chao, W.L., Harteneck, B.D., Liddle, J.A., Anderson, E.H., Attwood, D.T., 2005. Soft X-ray microscopy at a spatial resolution better than 15 nm. Nature 435, 1210–1213.

Daulton, T.L., Little, B.J., Lowe, K., Jones-Meehan, J., 2002. Electron energy loss spectroscopy techniques for the study of microbial chromium(VI) reduction. J. Microbiol. Methods 50, 39–54.

Drummy, L.F., Chen, J., Yang, J., Martin, D.C., 2006. Low voltage electron microscopy of organic materials. Microsc. Microanal. 12 (S2), 1436–1437.

Dynes, J.J., Tyliszczak, T., Araki, T., Lawrence, J.R., Swerhone, G.D.W., Leppard, G.G., Hitchcock, A.P., 2006a. Quantitative mapping of metal species in bacterial biofilms using scanning transmission X-ray microscopy. Environ. Sci. Technol. 40, 1556–1565.

Dynes, J.J., Lawrence, J.R., Korber, D.R., Swerhone, G.D.W., Leppard, G.G., Hitchcock, A.P., 2006b. Quantitative mapping of chlorhexidine in diatoms in natural river biofilms. Sci. Total Environ. 369, 369–383.

Egerton, R.F., 1996. EELS in the Electron Microscope, 2nd ed. Plenum, New York.
Feser, M., Beetz, T., Carlucci-Dayton, M., Jacobsen, C., 2000. Instrumentation advances and detector development with the Stony Brook scanning transmission X-ray microscope. AIP Conf. Proc. 507, 367–372.
Fiala, J.C., 2005. Reconstruct: a free editor for serial section microscopy. J. Microsc. 218, 52–61.
Fischer, P., Eimueller, T., Schutz, G., Bayreuther, G., Tsunashima, S., Takagi, N., Denbeaux, G., Attwood, D.T., 2001. Magnetic domains in nanostructured media studied with M-TXM. J. Synchrotron Radiat. 8, 325–327.
Guay, D., Stewart-Ornstein, J., Zhang, X., Hitchcock, A.P., 2005. In situ spatial and time resolved studies of electrochemical reactions by scanning transmission X-ray microscopy. Anal. Chem. 77, 3479–3487.
Hanhan, S., Obst, M., Dynes, J.J., Hitchcock, A.P., Kaznatcheev, K., Karunakaran, C., 2007. A liquid cell for solution and wet sample studies by STXM, 2005–2006 Canadian Light Source Report, pp. 117–119.
Hernández Cruz, D., Hitchcock, A.P., West, M.M., Rousseau, M.-E., Pézolet, M., 2006. Quantitative mapping of the orientation of fibroin β-sheets in *B. mori* cocoon fibers by scanning transmission X-ray microscopy. Biomacromolecules 7, 836–843.
Hernández-Cruz, D., Hitchcock, A.P., Tyliszczak, T., Rousseau, M.-E., Pézolet, M., 2007. In situ azimuthal rotation device for linear dichroism measurements in scanning transmission X-ray microscopy. Rev. Sci. Inst. 78, 033703-1-6.
Hitchcock, A.P., Araki, T., Ikeura-Sekiguchi, H., Iwata, N., Tani, K., 2003. 3D chemical mapping of toners by serial section scanning transmission X-ray microscopy. J. Phys. IV France 104, 509–512.
Hitchcock, A.P., Morin, C., Zhang, X., Araki, T., Dynes, J.J., Stover, H., Brash, J.L., Lawrence, J.R., Leppard, G.G., 2005. Soft X-ray spectromicroscopy of biological and synthetic polymer systems. J. Electron Spectrosc. Relat. Phenom. 144–147, 259–269.
Hitchcock, A.P., Johansson, G.A., Mitchell, G.E., Keefe, M., Tyliszcak, T., submitted for publication. 3D chemical imaging using angle-scan tomography in a soft X-ray scanning transmission X-ray microscope. Appl. Phys. A.
Horiuchi, S., Dohi, H., 2006. Nanoimaging and spectroscopic analysis of rubber/ZnO interfaces by energy-filtering transmission electron microscopy. Langmuir 22, 4607–4613.
Howells, M., Jacobsen, C., Warwick, T., 2007. Principles and Applications of Zone Plate X-Ray Microscopes in The Science of Microscopy. Kluwer Press.
Jin-Phillipp, N.Y., Rühle, M., 2004. Carbon nanotube/metal interface studied by cross-sectional transmission electron microscopy. Phys. Rev. B 70, 245421-1–245421-5.
Johansson, G.A., Tyliszczak, T., Mitchell, G.E., Keefe, M., Hitchcock, A.P., 2007. Three dimensional chemical mapping by scanning transmission X-ray spectromicroscopy. J. Synchrotron Radiat. 14, 395–412.
Kaznatcheev, K., Blomqvist, I., Hallin, E., Urquhart, S.G., Loken, D., Tylisczak, T., Warwick, T., Hitchcock, A.P., 2004. Principles of optical design of the SM beamline at the CLS. AIP Conf. Proc. 705, 1303–1307.
Kaznatcheev, K.V., Karunakaran, Ch., Lanke, U.D., Urquhart, S.G., Obst, M., Hitchcock, A.P., 2007. Soft X-ray spectromicroscopy beamline at the CLS: commissioning results. Nucl. Instrum. Methods 258 .
Kilcoyne, A.L.D., Tyliszczak, T., Steele, W.F., Fakra, S., Hitchcock, P., Franck, K., Anderson, E., Harteneck, B., Rightor, E.G., Mitchell, G.E., Hitchcock, A.P., Yang, L., Warwick, T., Ade, H., 2003. Interferometer-controlled scanning transmission X-ray microscopes at the Advanced Light Source. J. Synchrotron Radiat. 10, 125–136.
Kirz, J., Rarback, H., 1985. Soft X-ray microscopes. Rev. Sci. Instrum. 56, 1–13.
Kirz, J., Jacobsen, C., Howells, M., 1995. Soft X-ray microscopes and their biological applications. Q. Rev. Biophys. 28, 33–130.
Larabell, C.A., Le Gros, M.A., 2004. X-ray tomography generates 3D reconstructions of the yeast, *Saccharomyces cerevisiae*, at 60-nm resolution. Mol. Biol. Cell 15, 957–962.
Lawrence, J.R., Swerhone, G.D.W., Neu, T.R., 2000. Design and evaluation of a simple rotating annular reactor for replicated biofilm studies. J. Microb. Methods 42, 215–224.
Lawrence, J.R., Swerhone, G.D.W., Leppard, G.G., Araki, T., Zhang, X., West, M.M., Hitchcock, A.P., 2003. Scanning transmission X-ray, laser scanning, and transmission electron microscopy mapping of the exopolymeric matrix of microbial biofilms. Appl. Environ. Microbiol. 69, 5543–5554.
Leapman, R.D., Sun, S., 1995. Cryo-electron energy loss spectroscopy: observations on vitrified hydrated specimens and radiation damage. Ultramicroscopy 59, 71–79.
Libera, M., Disko, M.M., 2004. In: Ahn, C. (Ed.), Electron Energy Loss Spectroscopy of Polymers in Transmission Electron Energy Loss Spectrometry in Materials Science. Wiley-VCH, pp. 419–454.
London, R.A., Trebes, J.E., Jacobsen, C.J., 1992. The role of X-ray induced damage in biological microimaging. In: Jacobsen, C., Trebes, J. (Eds.), Soft X-ray Microscopy. Proc. SPIE 1741, 342–346.
Mastronarde, D.N., 1997. Dual-axis tomography: an approach with alignment methods that preserve resolution. J. Struct. Biol. 120, 343–352.
McDonald, C.J., Devon, M.J., 2002. Hollow latex particles: synthesis and applications. Adv. Colloid Interface Sci. 99, 181–213.
Rightor, E.G., Hitchcock, A.P., Ade, H., Leapman, R.D., Urquhart, S.G., Smith, A.P., Mitchell, G.E., Fischer, D., Shin, H.J., Warwick, T., 1997. Spectromicroscopy of poly(ethylene terephthalate): comparison of spectra and radiation damage rates in X-ray absorption and electron energy loss. J. Phys. Chem. B 101, 1950–1961.
Rousseau, M.-E., Hernández Cruz, D., West, M.M., Hitchcock, A.P., Pézolet, M., 2007. *Nephilia clavipes* spider dragline silk microstructure studied by scanning transmission X-ray microscopy. J. Am. Chem. Soc. 129, 3897–3905.
Schmahl, G., Rudolph, D., Niemann, B., Christ, O., 1980. Zone-plate X-ray microscopy. Q. Rev. Biophys. 13, 297–315.
Sigle, W., 2005. Analytical transmission electron microscopy. Ann. Rev. Mater. Res. 35, 239–314.
Sousa, A., Aitouchen, A., Libera, M., 2006a. Water mapping of hydrated soft matter. Ultramicroscopy 106, 130–145.
Sousa, A., Sengonul, M., Latour, R., Kohn, J., Libera, M., 2006b. Selective protein adsorption on a phase-separated polymer blend. Langmuir 22, 6286–6292.
Spence, J.C.H., 2006. Absorption spectroscopy with sub-angstrom beams: ELS in STEM. Rep. Prog. Phys. 69, 725–758.
Stéphan, O., Kociak, M., Henrard, L., Suenaga, K., Gloter, A., Tencé, M., Sandré, E., Colliex, C., 2001. Electron energy-loss spectroscopy on individual nanotubes. J. Electron Spec. Relat. Phenom. 114, 209–217.
Wang, Y., Jacobsen, C., Maser, J., Osanna, A., 2000. Soft X-ray microscopy with a cryo STXM: II. Tomography. J. Microsc. 197, 80–93.